

# Coupling Quantum Emitters in WSe<sub>2</sub> Monolayers to a Metal-Insulator-Metal Waveguide

*Subhajit Dutta,<sup>a</sup> Tao Cai,<sup>a</sup> Mustafa Atabey Buyukkaya,<sup>a</sup> Sabyasachi Barik,<sup>a,b</sup> Shahriar Aghaeimeibodi,<sup>a</sup> Edo Waks<sup>a,b</sup>*

<sup>a</sup> Department of Electrical and Computer Engineering and Institute for Research in Electronics and Applied Physics, University of Maryland, College Park, Maryland 20742, USA.

<sup>b</sup> Joint Quantum Institute, University of Maryland and the National Institute of Standards and Technology, College Park, Maryland 20742, USA.

\* Corresponding author E-mail: [edowaks@umd.edu](mailto:edowaks@umd.edu)

**ABSTRACT:** Coupling single photon emitters to surface plasmons provides a versatile ground for on chip quantum photonics. However, achieving good coupling efficiency requires precise alignment of both the position and dipole orientation of the emitter relative to the plasmonic mode. We demonstrate coupling of single emitters in the 2-D semiconductor, WSe<sub>2</sub> self-aligned with propagating surface plasmon polaritons in silver-air-silver, metal-insulator-metal waveguides. The waveguide produces strain induced defects in the monolayer which are close to the surface plasmon mode with favorable dipole orientations for optimal coupling. We measure an average Purcell factor of 1.8 for coupling the single defects to the plasmonic waveguide. This architecture provides an efficient way of coupling single photon emitters to propagating plasmons which is an important step towards realizing active plasmonic circuits on chip.

In recent years, defects bound excitons in two dimensional semiconductors have emerged as a new class of single photon emitters with ultra-narrow linewidths of 100  $\mu$ eVs, as well as high single photon purity.<sup>1-4</sup> These emitters are located at the surface of an atomically thin monolayer which allows them to come in close proximity to photonic nanostructures. Another characteristic feature is that they can be deterministically induced by strain engineering allowing for site specific positioning.<sup>5-7</sup> Thus, with the ability to position these atomically thin quantum emitters, one can efficiently couple to the confined mode of optical nanostructures providing a platform for coherent light-matter interactions. Such a platform is critical for applications such as quantum communication and quantum information processing<sup>8,9</sup>.

2D materials with their narrow linewidths and flexibility in terms of positioning, offer a promising path to tailoring strong light matter interactions. However, apart from nanoscale positioning of emitters, the nanostructure must also exhibit a high optical density of states. A strong contender for the photonic nanostructures are surface plasmon polaritons generated at a metal-dielectric interface. Surface plasmons exhibit extreme subwavelength confinement of light<sup>10,11</sup> and an atom-like dipole emitter placed near the metal-dielectric interface, preferentially emits into the

surface plasmon mode due to its high optical density of states.<sup>12</sup> The strong optical decay of emitters into the surface plasmon results in efficient coupling of emitters to a common plasmonic mode that can lead to strong photon-photon interactions.<sup>13</sup> Coupling also produces a significant enhancement in the rate of spontaneous emission of the emitters<sup>12,14,15</sup> which can help realize a fast single photon source on-chip. Thus, single photon emitters in 2D materials, coupled to surface plasmon polaritons establishes a platform for compact active photonic circuits essential for quantum information processing<sup>16-18</sup>.

Several previous works report deterministic coupling of quantum emitters with plasmonic nanocavities<sup>19-21</sup>. However, this does not realize a propagating surface plasmon polariton which is desirable for non-linear plasmonic circuit elements. More recent work realizes a travelling mode by coupling single localized defects in a WSe<sub>2</sub> monolayer self-aligned to the propagating surface plasmon mode of a silver nanowire.<sup>22</sup> These emitters however, show no significant radiative enhancement, because the electric field vector of the plasmonic mode is perpendicular to the metal surface and directed radially outward from the cylindrical metal nanowires, whereas single emitters in 2D materials have in plane dipole moments<sup>1-4</sup> which are tangential to the metal surface. Thus, dipole emitters in a monolayer placed on top of a nanowire waveguide have an unfavorable alignment to the local electric field vector. Metal-Insulator-Metal (MIM) waveguides solve this problem because the electric field of the surface plasmon has a strong in-plane component that is perpendicular to the metal surface.

Here we show coupling of single emitters in WSe<sub>2</sub> with a propagating surface plasmon polaritons in silver-air-silver, MIM waveguides. The strain gradient enforced on the monolayer by the waveguide generates sharp localized single photon emitters close to the plasmonic mode. The component of the in-plane dipole moment perpendicular to the metal surface preferentially couples to the travelling waveguide mode, leading to a Purcell enhanced emission with an average Purcell factor of 1.8. A single emitter in a 2D material coupled to an MIM waveguides can lead to deterministic active plasmonic circuits that can be lithographically fabricated on chip.

Figure 1. shows a finite-difference time-domain simulation for the surface plasmon mode in a silver-air-silver MIM structure. The color map represents the magnitude of the electric field ( $E_x$ ) vector of the plasmon polariton mode, directed along the X axis which is oriented in the in-plane direction. This electric field component exhibits a strong localization in the air gap region between the two metal strips of the MIM waveguide. Because the monolayer dipole moment is in-plane, it can align to the electric field orientation of the waveguide. This contrasts with nanowire waveguides where the preferred dipole orientation is radial to the structure and always orthogonal to the plane of the monolayer, hampering coupling efficiency.

We fabricate the MIM waveguides using electron beam lithography, followed by metal deposition and liftoff. We spin coat Si/SiO<sub>2</sub> sample with ZEP520A ebeam resist at 4500 rpm and post bake it for 5 min at 180° C. Next, we pattern the samples using an electron beam lithography system at an acceleration voltage of 100 kV (Elionix ELS-G100), using a dose array ranging from 250 to 480  $\mu$ C/cm<sup>2</sup>. We develop the resist in n-Amyl Acetate (ZED-N50), Methyl isobutyl ketone and Isopropyl alcohol for 1min, 30s and 30s respectively. For the metal evaporation step, we use a thermal evaporator to deposit 5nm and 65nm, Cr and Ag at evaporation rates of 5 A/s and 130

A/s, respectively to achieve high quality plasmonic films.<sup>23</sup> We perform liftoff by soaking in acetone overnight and subsequently rinsing with Acetone and Isopropyl alcohol. The fabricated waveguides have gaps ranging from 90 nm to 110 nm and a length of 7  $\mu\text{m}$ , Fig. 2(a). After waveguide fabrication, we transfer the monolayer samples onto the MIM structures. We grow WSe<sub>2</sub> monolayers on a sapphire substrate using a chemical vapor deposition method<sup>24</sup> and then dry stamp them on the MIM sample using a polydimethylsiloxane (PDMS) gel as an intermediate transfer medium.<sup>25</sup>

To characterize the sample, we cool it to 3.2 K in closed cycle cryostat (Attocube Inc.) and perform photoluminescence measurements using a confocal microscope geometry. We use a continuous wave excitation laser emitting at 532 nm to perform photoluminescence spectroscopy. We focus the laser onto the sample surface with an objective lens (Numerical aperture 0.7) to excite a small diffraction limited spot on the MIM waveguide. A 700 nm long-pass optical filter rejects the pump wavelength to isolate the fluorescence signal. A monochrome scientific camera (Rolera-XR, Qimaging, Inc.) images the fluorescence field pattern. Alternately, we use a grating spectrometer (SP2750, Princeton Instruments) to measure the fluorescence spectrum.

Fig. 2(b) shows the photoluminescence image of the MIM waveguide as observed on the camera. We observe bright localized emission spots in the vicinity of the waveguide. The photoluminescence spectrum, Fig. 2(c) of the bright spot as marked in the figure (dotted circle) shows the presence of several sharp peaks corresponding to single defects emitters in WSe<sub>2</sub>.<sup>1-4</sup> These emitters arise from the strain gradient affected on the monolayer by the MIM waveguide. Such strain-induced defect formations have been previously shown in monolayers suspended over holes or placed on top of nanopillars and nanowires.<sup>5,7,22</sup> We further observe bright spots at the ends of the waveguide. We assert that the emission from these single defects couple to the propagating surface plasmon polariton in the waveguide and scatter at the ends as photons resulting in such bright spots.

To verify the assertion of coupling, we search along the waveguide for defects while looking for scattered emission at the ends. Fig. 3(a) shows a camera image of the fluorescence intensity when we excite point A near one end of a waveguide. The corresponding spectrum shows two resolvable peaks at 736.6 nm and 737.1 nm which are labelled as Z and X, respectively in Fig 3(b). We fit the peaks to a Lorentzian to determine linewidths of 0.17 nm (Z) and 0.10 nm (X). These peaks constitute a set of orthogonally polarized doublets.<sup>1-4</sup> Keeping the excitation at A we move the collection spot to the point B at the far end of the waveguide and collect the corresponding spectrum. This time we observe only one of the doublet peaks at 737.4 nm because only one of the two cross polarized peaks aligns with the direction of the electric field of the surface plasmon polariton. The peak vanishes when we move the excitation spot away from A. To ensure that the emission we see is not due to the pump coupling to the waveguide and exciting a different defect at the other end, we directly excite B with a laser and measure the emission at the same point. The spectrum, shown in Fig. 3(d), displays the broad background photoluminescence emission from the monolayer flake and does not show the sharp peak observed when exciting point A.

Spontaneous emission enhancement is a strong signature of efficient coupling of dipole emitters to optical nanostructures. But measuring radiative enhancement in WSe<sub>2</sub> emitters is complicated by the fact that even in pristine monolayer, the radiative lifetimes are broadly distributed and can range from 3 ns to as long as 19 ns.<sup>21</sup> To explore Purcell enhancement, we therefore accumulate statistics over a total of 17 emitters, with 7 emitters located on the waveguide/monolayer system and 10 emitters located on the pristine monolayer, away from the waveguide. The distributions of the radiative lifetimes for the two sets of emitters are plotted in Fig. 4(b) and (c). We see a clear decrease of the lifetimes for the emitters that are located on the MIM waveguide. The average radiative lifetime of these emitters turns out to be 3.34 ns while that of the emitters in the pristine flake is 6 ns. From these values we determine an average Purcell enhancement of 1.8 for near-field coupling of the single emitters to the MIM waveguides.

In conclusion, we showed coupling of single emitters in WSe<sub>2</sub> with propagating surface plasmon polaritons in MIM waveguides. The strain gradient enforced on the monolayer by the waveguide generated localized single photon emitters close to the plasmonic mode. The coupled emitters experienced an enhancement in the radiative lifetime measured by the average Purcell factor of 1.8. Our results can realize a fast, integrated single photon source by coupling the MIM structure with a dielectric waveguide.<sup>26,27</sup> It is however, necessary to gain better control over the coupling strength between the emitter and the plasmonic mode. One approach might be to engineer better quality of defects by reducing the non-radiative relaxation in the system by encapsulating the monolayer by boron nitride layers<sup>28</sup> which is known to decrease the linewidths of the defects. With better control over the coupling strength one can think of more appealing applications that harp on the giant non-linearity presented by the plasmon-emitter system. The saturable two-level system of the emitter absorbs and subsequently scatters off single photons while being invisible to the next photon. This can realize a single photon switch.<sup>18</sup> Thus, combined with recent advances in the fabrication quality of 2D monolayer,<sup>28</sup> our results present a versatile platform which can lead to compact active plasmonic circuits on chip.

**Acknowledgements:** The authors acknowledge support from the National Science Foundation (award number ECCS1508897), the Office of Naval Research ONR (award number N000141410612), the Air Force Office of Scientific Research (AFOSR) (award number 271470871D), and the Physics Frontier Center at the Joint Quantum Institute.

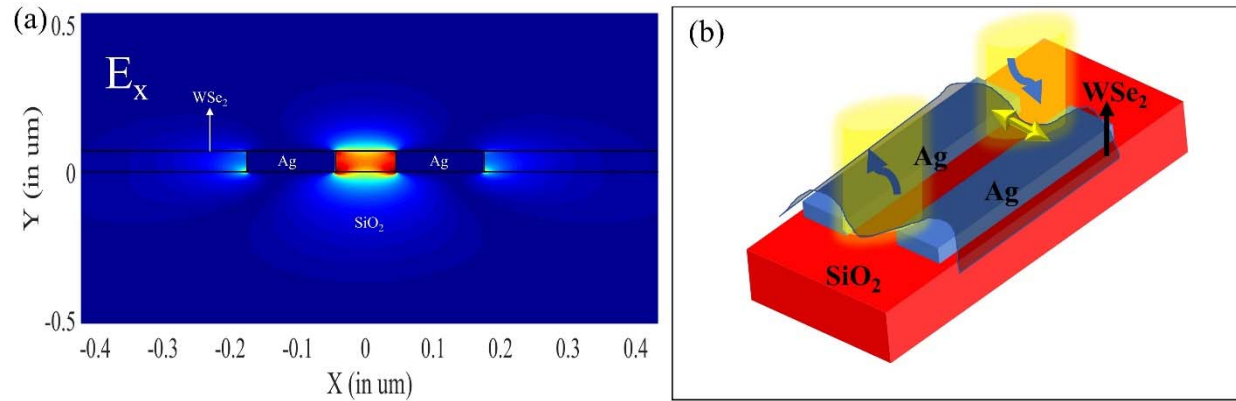


Fig. 1. (a) FDTD simulation showing the X component of the electric field for the surface plasmon mode propagating along the Z axis in the MIM waveguide. (b) Schematic of an MIM waveguide covered by a WSe<sub>2</sub> monolayer. The green dipole represents a quantum emitter in WSe<sub>2</sub>. The blue arrows denote the excitation and collection points respectively.

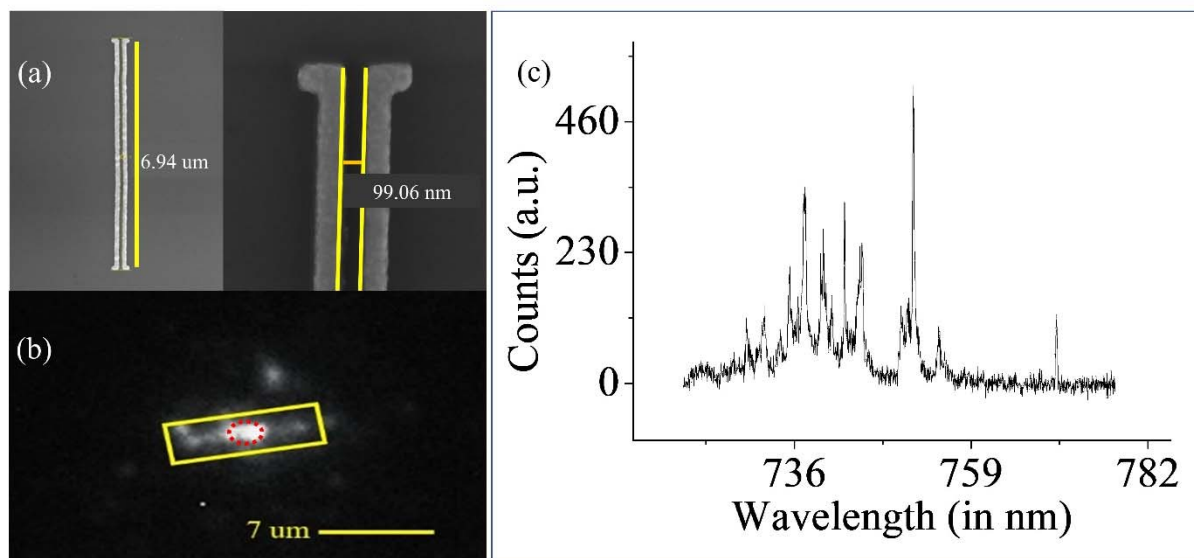


Fig. 2. (a) SEM image of a representative MIM waveguide showing the length and gap width. (b) Shows the PL of a WSe<sub>2</sub> flake located on top of a waveguide marked by the yellow box. (b) PL spectrum collected at the point on the waveguide marked by the dotted circle showing multiple defect emissions structurally aligned with the waveguide.

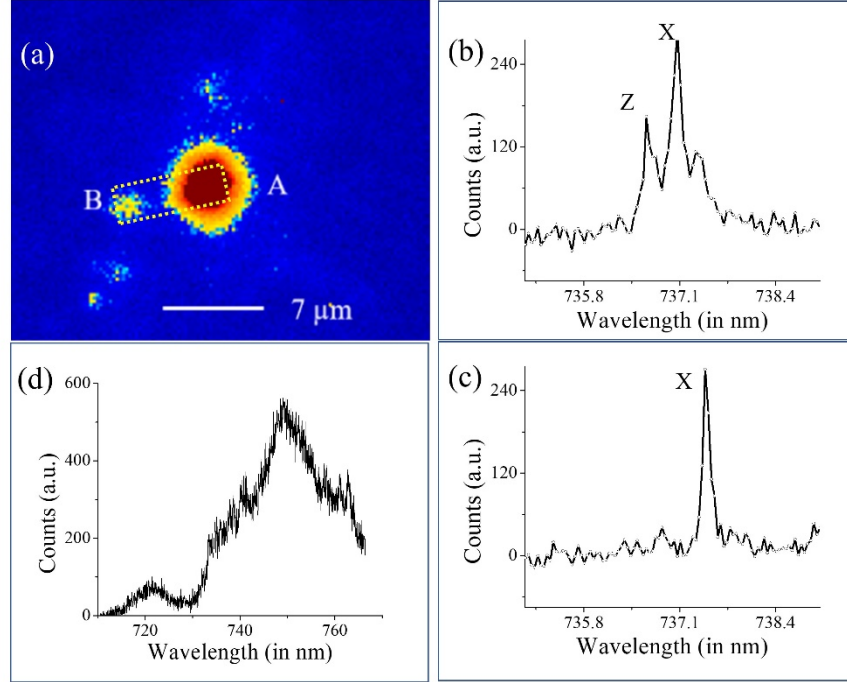


Fig. 3. (a) Shows the photoluminescence spectrum of a defect at A (Point near one end of the MIM waveguide) being waveguided and scattered off the end, B. (The far end of the waveguide) (b) Shows the photoluminescence spectrum with the excitation and collection at A. X and Z correspond to an orthogonally polarized doublet polarized along the X and Z axes respectively. (c) Shows the photoluminescence spectrum of the waveguided defect, X when the excitation is at A and the collection is at B. (d) Shows the photoluminescence spectrum when both the excitation and collection are aligned to point B.

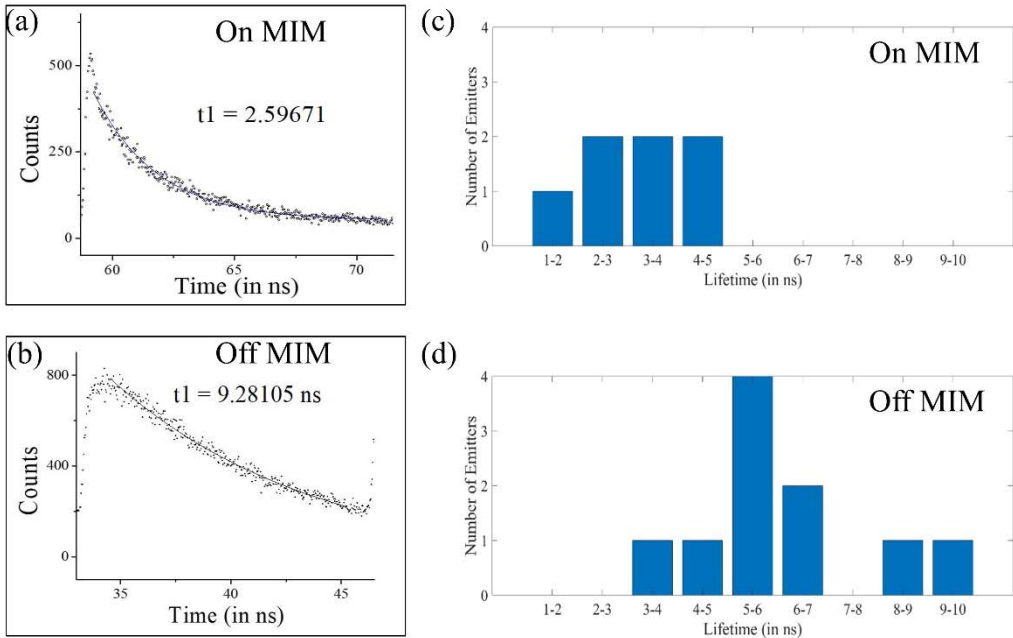


Fig. 4. (a) Lifetime of a representative emitter located on the MIM waveguide. (b) Lifetime of a representative emitter located away from the MIM waveguide. (c) Lifetime statistics of emitters located near the waveguide. (d) Lifetimes of emitters located far from the waveguide.

<sup>1</sup> Y.M. He, G. Clark, J.R. Schaibley, Y. He, M.C. Chen, Y.J. Wei, X. Ding, Q. Zhang, W. Yao, X. Xu, C.Y. Lu, and J.W. Pan, *Nat. Nanotechnol.* **10**, 497 (2015).

<sup>2</sup> C. Chakraborty, L. Kinnischtzke, K.M. Goodfellow, R. Beams, and A.N. Vamivakas, *Nat. Nanotechnol.* **10**, 507 (2015).

<sup>3</sup> M. Koperski, K. Nogajewski, A. Arora, V. Cherkez, P. Mallet, J.Y. Veuillen, J. Marcus, P. Kossacki, and M. Potemski, *Nat. Nanotechnol.* **10**, 503 (2015).

<sup>4</sup> A. Srivastava, M. Sidler, A. V. Allain, D.S. Lembke, A. Kis, and A. Imamoglu, *Nat. Nanotechnol.* **10**, 491 (2015).

<sup>5</sup> C. Palacios-Berraquero, D.M. Kara, A.R.P. Montblanch, M. Barbone, P. Latawiec, D. Yoon, A.K. Ott, M. Loncar, A.C. Ferrari, and M. Atatüre, *Nat. Commun.* **8**, 1 (2017).

<sup>6</sup> J. Kern, I. Niehues, P. Tonndorf, R. Schmidt, D. Wigger, R. Schneider, T. Stiehm, S. Michaelis de Vasconcellos, D.E. Reiter, T. Kuhn, and R. Bratschitsch, *Adv. Mater.* **28**, 7101 (2016).

<sup>7</sup> S. Kumar, A. Kaczmarczyk, and B.D. Gerardot, *Nano Lett.* **15**, 7567 (2015).

<sup>8</sup> H.J. Kimble, *Nature* **453**, 1023 (2008).

<sup>9</sup> C. Monroe, *Nature* **416**, 238 (2002).

<sup>10</sup> W.L. Barnes, A. Dereux, and T.W. Ebbesen, *Nature* **424**, 824 (2003).

<sup>11</sup> J.A. Schuller, E.S. Barnard, W. Cai, Y.C. Jun, J.S. White, and M.L. Brongersma, *Nat. Mater.* **9**, 193 (2010).

<sup>12</sup> A. Huck and U.L. Andersen, *Nanophotonics* **5**, 1 (2016).

<sup>13</sup> V.N. Pustovit and T. V. Shahbazyan, *Phys. Rev. Lett.* **102**, 1 (2009).

<sup>14</sup> T.B. Hoang, G.M. Akselrod, and M.H. Mikkelsen **16**, 270 *Nano Lett.* (2016).

<sup>15</sup> K. Matsuzaki, S. Vassant, H.W. Liu, A. Dutschke, B. Hoffmann, X. Chen, S. Christiansen, M.R. Buck, J.A. Hollingsworth, S. Götzinger, and V. Sandoghdar, *Sci. Rep.* **7**, 1 (2017).

<sup>16</sup> D.E. Chang, A.S. Sørensen, P.R. Hemmer, and M.D. Lukin, *Phys. Rev. Lett.* **97**, 1 (2006).

<sup>17</sup> J.M. Fitzgerald, P. Narang, R. V. Craster, S.A. Maier, and V. Giannini, *Proc. IEEE* **104**, 2307 (2016).

<sup>18</sup> D.E. Chang, A.S. Sørensen, E.A. Demler, and M.D. Lukin, *Nat. Phys.* **3**, 807 (2007).

<sup>19</sup> M. Nguyen, S. Kim, T.T. Tran, Z.-Q. Xu, M. Kianinia, M. Toth, and I. Aharonovich, *Nanoscale* **10**, (2018).

<sup>20</sup> T.T. Tran, D. Wang, Z.Q. Xu, A. Yang, M. Toth, T.W. Odom, and I. Aharonovich, *Nano Lett.* **17**, 2634 (2017).

<sup>21</sup> L.N. Tripathi, O. Iff, S. Betzold, M. Emmerling, K. Moon, Y.J. Lee, S.-H. Kwon, S. Höfling, and C. Schneider **5**, 1919 (2017).

<sup>22</sup> T. Cai, S. Dutta, S. Aghaeimeibodi, Z. Yang, S. Nah, J.T. Fourkas, and E. Waks, *Nano Lett.* **17**, 6564 (2017).

<sup>23</sup> K.M. McPeak, S. V. Jayanti, S.J.P. Kress, S. Meyer, S. Iotti, A. Rossinelli, and D.J. Norris, *ACS Photonics* **2**, 326 (2015).

<sup>24</sup> J. K. Huang, J. Pu, C. L. Hsu, M. H. Chiu, Z. Y. Juang, Y. H. Chang, W. H. Chang, Y. Iwasa, T. Takenobu, and L. J. Li, *ACS Nano* **8**, 923 (2014).

<sup>25</sup> A. Castellanos-Gomez, M. Buscema, R. Molenaar, V. Singh, L. Janssen, H.S.J. Van Der Zant, and G.A. Steele, *2D Mater.* **1**, (2014).

<sup>26</sup> G. Veronis and S. Fan, *Opt. Express* **15**, 1211 (2007).

<sup>27</sup> R. Yang, R.A. Wahsheh, Z. Lu, and M.A.G. Abushagur, *Opt. Lett.* **35**, 649 (2010).

<sup>28</sup> O. A. Ajayi, J. V. Ardelean, G. D. Shepard, J. Wang, A. Antony, T. Taniguchi, K. Watanabe, T. F. Heinz, S. Strauf, X.-Y. Zhu, and J. C. Hone, *2D Mater.* **4**, 031011 (2017).